7-2024

Study of structural, electronic, optical and mechanical properties of K2ScCuF6 and K2YCuF6 perovskites via DFT calculations

Amina --

Muhammad Uzair

Amir Sohail Khan

A.M. Quraishi

Albandary Almahri

See next page for additional authors

Authors

Amina --, Muhammad Uzair, Amir Sohail Khan, A.M. Quraishi, Albandary Almahri, Mukhlisa Soliyeva, Vineet Tirth, Ali Algahtani, Abdullah --, Rawaa M. Mohammed, Mahidur R. Sarker, N.M.A. Hadia, and Abid Zaman

Results in Physics 62 (2024) 107845

Contents lists available at ScienceDirect

Results in Physics

journal homepage: www.elsevier.com/locate/rinp

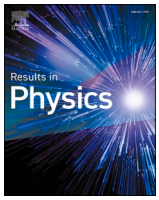

Study of structural, electronic, optical and mechanical properties of K_2ScCuF_6 and K_2YCuF_6 perovskites via DFT calculations

Amina [a,*], Muhammad Uzair [b], Amir Sohail Khan [c], A.M. Quraishi [d], Albandary Almahri [e], Mukhlisa Soliyeva [f], Vineet Tirth [g,h], Ali Algahtani [g,h], Abdullah [i], Rawaa M. Mohammed [j], Mahidur R. Sarker [k,l], N.M.A. Hadia [m], Abid Zaman [n,*]

[a] Department of Physics, Bacha Khan University Charsadda, Pakistan
[b] Department of Physics, University of Peshawar, Peshawar, 25120, KP, Pakistan
[c] Department of Energy Systems Research, Ajou University, Suwon, 16499, Republic of Korea
[d] Department of Electrical Engineering, College of Engineering, Qassim University, Buraydah. 51452, Saudi Arabia
[e] Department of Chemistry, College of Science and Humanities in Prince Sattam Bin Abdulaziz University Al-Kharj 11942, Saudi Arabia
[f] Department of Physics and Teaching Methods, Tashkent State Pedagogical University, Tashkent, Uzbekistan
[g] Mechanical Engineering Department, College of Engineering, King Khalid University, Abha 61421, Asir, Kingdom of Saudi Arabia
[h] Research Center for Advanced Materials Science (RCAMS), King Khalid University, Guraiger, Abha-61413, Asir, Kingdom of Saudi Arabia
[i] Department of Physics, Government Post Graduate College Karak, 27200 Pakistan
[j] Ph.D in clinical microbiology, College of Nursing, Al-Mustaqbal University, Iraq
[k] Institute of Visual Informatics, Universiti Kebangsaan Malaysia, Bangi 43600, Selangor, Malaysia
[l] Universidad de Diseño, Innovación y Tecnología, UDIT, Av. Alfonso XIII, 97, 28016 Madrid, Spain
[m] Department of Physics, College of Science, Jouf University, Sakaka 2014, Al-Jouf, Saudi Arabia
[n] Department of Physics, Riphah International University Islamabad 44000, Pakistan

ARTICLE INFO

Keywords:
Density Functional Theory
Pb-free Double perovskite
Opto-electronic properties
Elastic behaviors

ABSTRACT

Owing to their outstanding performance, environmental friendliness and stability, perovskite materials are becoming very important for solar cells, renewable energy sources and thermoelectric generators. This work uses the first-principles approach to explore the structural, electronic, optical and elastic characteristics of K_2ScCuF_6 and K_2YCuF_6 double perovskites. The negative formation energy in Birch-Murnaghan confirms the stability of the compounds in Fm3m (225) space group. The analysis of the electronic properties concluded that both K_2ScCuF_6 and K_2YCuF_6 are narrow band gap semiconductors materials, having 1.2 and 2.3 eV of bandgap energies, respectively. This was further verified by the density of states. The mechanical stability, ductility and anisotropic nature of the compounds was shown by analyzing their elastic constants. In addition, the optical properties showed transparency at low energy values but showed both transmission and absorption characteristics at higher energy levels. These interesting results imply that K_2ScCuF_6 and K_2YCuF_6 have significant potential in solar cells, light-emitting diodes (LEDs), smart windows, displays and sensors.

Introduction

The switch to renewable energy sources and a revolution in energy conversion storage techniques are essential owing to the present energy challenges, climate change, and decline of fossil fuel supplies [1–3]. The fact that solar energy is widely available and reasonably priced makes it an excellent alternative [4,5]. To develop solar cells that are both cost-effective and efficient, research and innovation is still needed [6,7]. Numerous materials are being studied to identify novel materials with distinctive features [8,9]. Double Perovskites have been proved to have these significant features which has the potential to fascinate the researchers to investigate its properties [8–12].

Double perovskites have a unique structure such as $A_2BB'X_6$, where A and B/B' are cations and X is anion [13,14]. By adjusting the component elements and their corresponding oxidation states, this complex arrangement allows double perovskites to have exceptionally flexible material characteristics. By learning more about the double perovskites and design elements of solar cells, we aim to advance solar

* Corresponding authors.
E-mail addresses: dramina.faculty@bkuc.edu.pk (Amina), zaman.abid87@gmail.com (A. Zaman).

https://doi.org/10.1016/j.rinp.2024.107845
Received 22 May 2024; Received in revised form 17 June 2024; Accepted 20 June 2024
Available online 22 June 2024

cell technology and get closer to the goal of economical and efficient solar energy conversion [15–19]. The organic–inorganic hybrid lead-based compounds have shown high efficiency up to 22 % in double perovskites ($CH3NH3Pb_{1-x}Cu_xBr3$ and $CH3NH3PbX_3$; X = I, Br, and Cl); nevertheless, they suffer from lead toxicity and instability under ambient conditions. To mitigate these concerns in perovskite structures, researchers are now looking for substitute elements [20–26]. Group IV elements of the same family (Sn, Ge) are thought to be a viable replacement for Pb in perovskite materials [27,28]. However, the substitution of Sn results in efficiency drops by 10 %, quick oxidization, possible health risks and Ge results in oxidization shifts to + 4 from + 2 states, which causes the materials to decompose quickly [29]. Alternatively, more stable elements such as Cs, Ag, Na, K, Cu, Bi, Sb, In, Fe, Ti, Pd, etc., have been studied to develop variety of lead-free perovskites or derivatives, including distinct perovskite structures and halide double perovskites [30]. Researchers from halide perovskite community recently suggested semiconductor compounds as a substitute substance that is highly stable, less toxic, and illuminates at a high intensity. This proposal sparked renewed interest in halide double perovskites, a class of quaternary materials [13,31–33].

Recently, M. Shihab Uddin *et.al.* studied the $Cs_2AgBiBr_6$ and reported that it has band of 1.6 eV and exhibit UV absorption peaks around 15 eV intensifying with photon energy up to 3.75 eV, hinting at its promise for solar applications [34]. Furthermore, $CaPd_3V_4O_{12}$ is investigated and reported that the Fermi surface of $CaPd_3V_4O_{12}$ ensures a kind of hole as well as electron faces simultaneously, indicating multifarious band characteristics. The prediction of the static real dielectric function (optical property) of $CaPd_3V_4O_{12}$ at zero energy implies its promising dielectric nature [35]. Beside this photovoltaic (PV) performance of Cs_2BiAgI_6 double perovskite is enhanced by optimizing the optoelectronic parameters of the absorber, electron transport layer (ETL), hole transport layer (HTL), and various interface layers [36].

Research on the ideal material design and band gap engineering for solar cells and other applications is being conducted both computationally and experimentally [37–39]. Researchers often utilize computer simulations as a guide for modeling the most effective approaches to achieve their goals. This impetus strengthened our motivation to create materials for applications involving renewable energy. In this work, we investigated the structural, electronic, elastic and optical properties of K_2ScCuF_6 and K_2YCuF_6 compounds via density functional theory (DFT) specifically emphasizing how well suited they are for solar cells. To best our knowledge there is no study present regarding these materials. The structural and mechanical stability demonstrates its potential for solar cell applications. Therefore, we believe that our study would offer a solid foundation and adequate acknowledgment of utilizing such compounds for energy systems.

Computational methodology

A computational approach known as density functional theory (DFT) can be used to determine various material characteristics essential to comprehend how these materials behave and enhance their performance for practical manufacturing process [40]. To compute the characteristics of K_2ScCuF_6 and K_2YCuF_6 compounds in this work, we utilize the WIEN2k code [41]. We use the Murnaghan equations of state (EoS) to find optimal lattice parameters as well as energy of the system [42]. To fully optimize the structure force convergence criterion is taken 0.001 eV/ Å while the enrgy is converged up to 10^{-6} eV. Phonopy code is used to calculate the phonon dispersion curve. For phonon dispersion curve the supercell of 3 × 3 × 3 with K-mesh of 5 × 5 × 5 is used. The band gaps are determined with the help of well-known TB-mBJ potential, known for its precision and simplicity [43]. Elastic constants from IR-Elast package are used to study the elastic properties [44]. In order to ensure that the results of the calculations are accurate, a larger K-mesh (2000) is used to ensure that the charge and energy converge. In WIEN2k, −6.0 Ry is the energy below, treated as core states, assuming no interaction between core electrons. Furthermore, G_{max} of 12 and $R_{MT}K_{max}$ is 8 considered throughout the calculations.

Results and discussion

Structural properties

Two double perovskite structures from $Fm\bar{3}m$ (225) space group can be combined to form double perovskites K_2ScCuF_6 and K_2YCuF_6 of cubic structure given in Fig. 1. The polyhedral structure of compound K_2ScCuF_6 and K_2YCuF_6 indicates the formation of octahedra, inside which the atoms of the Cu and Sc/Y octahedra are positioned, and each octahedra atom is surrounded by six F atoms. The particular Wyckoff positions of the atoms K, Sc/Y, Cu, and F are (1/4, 3/4, 3/4), (0, 0, 0), (1/2, 0, 0), and (0.24, 0, 0)/ (0.274, 0, 0), respectively. The optimization procedure is carried out for both compounds to find the lowest volume that corresponds to the energy of the ground state of the unit cell and other lattice parameters shown in Table 1. Fig. 2 shows the volume optimization for the given double perovskite compounds. The parabolic curves explain how energy and volume are related to one another. The most stable configuration of the compounds is shown by the minimal points of these curves corresponding to their ground state.

Table 1 shows structural parameters and atomic sites of the unit cell which are necessary to understand the structural properties of the compounds. Bulk modulus indicates how resistant a material is to uniform compression and is dependent on the crystal's structure and chemical composition. It describes the hardness of the compound. Table 1 shows that K_2ScCuF_6 will take more energy to compress because it has a higher bulk modulus (B_o) compared to K_2YCuF_6. To check the dynamic stability, we calculated the phonon dispersion curve of both materials (K_2ScCuF_6 and K_2YCuF_6). The obtained results are shown in Fig. 3 (a&b). From figure it can be observed that there are no imaginary peaks indicating its dynamic stability.

Elastic properties

Analyzing a material's behavior under stress requires taking into account its mechanical stability as one of its most significant characteristics. The elastic constants, which express how a material responds to applied forces, can be used to determine mechanical stability. In particular, materials with cubic symmetry require three elastic constants (C_{11}, C_{12}, and C_{44}). The computed elastic constant values for the double perovskites K_2ScCuF_6 and K_2YCuF_6 are given in Table 2. The Born-Haun stability criteria, which include $C_{11} > 0$, $C_{11} - C_{12} > 0$, $C_{11} + 2\,C_{12} > 0$, $C_{12} < B < C_{11}$, and $C_{44} > 0$, are assessed for elastic constants in order to confirm the mechanical stability [45]. Given that the calculated elastic constants satisfy the conditions necessary for cubic crystals' mechanical stability, these compounds are therefore mechanically stable and won't collapse under the influence of interactions involving external stresses [46].

In Table 2, bulk modulus (B), shear modulus (G), Voigt shear modulus (G_v), Reuss shear modulus (G_R), anisotropy (A), Young's modulus (E), Poisson's ratio (ν), Pugh's ratio (B/G) were calculated via following equations [45,47]:

$$B = \frac{C_{11} + 2C_{12}}{3} \tag{1}$$

$$G = \frac{G_v + G_R}{2} \tag{2}$$

$$G_v = \frac{C_{11} + 3C_{44} - C_{12}}{5} \tag{3}$$

$$G_R = \frac{5(C_{11} - C_{12})C_{44}}{3(C_{11} - C_{12}) + 4C_{44}} \tag{4}$$

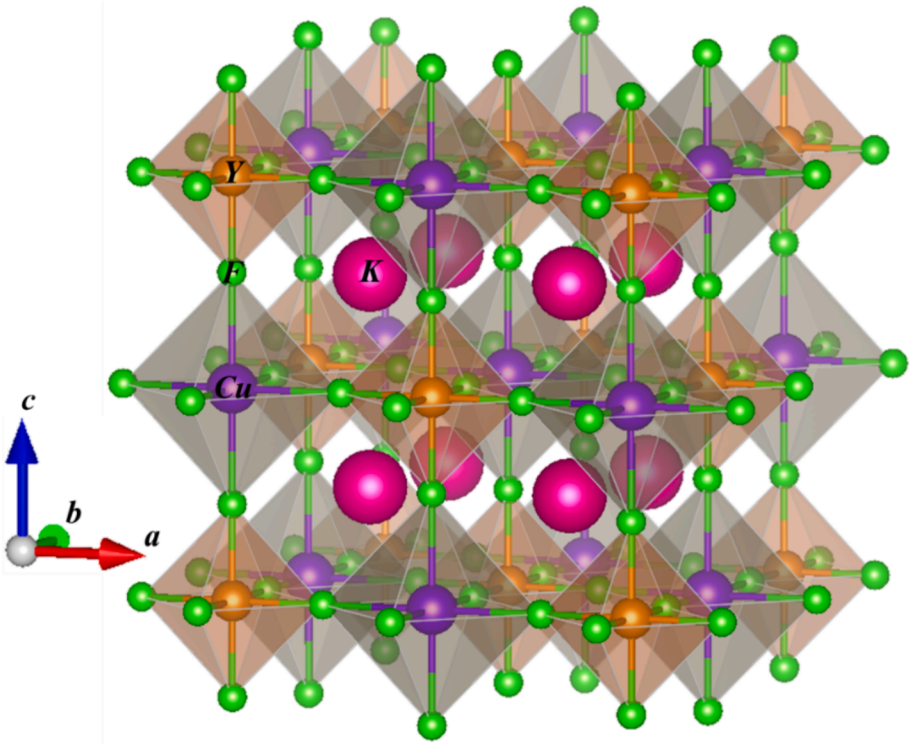

Fig. 1. Schematic structure of K_2YCuF_6 double perovskite compound.

Table 1
Calculated Structural Parameters of K_2ScCuF_6 and K_2YCuF_6.

Compound	$a_0/b_0/c_0$	α/β/γ	B_0 (GPa)	B′ (GPa)	E_0 (Ry)	V_0 (a.u)^3
K_2ScCuF_6	10.25 Å	90°	65.25	4.94	−8446.86	1051.07
K_2YCuF_6	10.30 Å	90°	54.81	4.84	−13689.82	1221.03

$$E = \frac{9GB}{3B + G} \tag{5}$$

$$A = \frac{2C_{44}}{C_{11} - C_{12}} \tag{6}$$

$$\nu = \frac{3B - 2G}{2(2B + G)} \tag{7}$$

Compressibility and stiffness of a material may be determined using two notable modules: bulk (B) and shear (G). The capacity of a material to resist to fracture is evaluated by B, whereas its capacity to withstand to plastic deformation is measured by G [48]. It is evident from the computed values shown in Table 2.1 that K_2ScCuF_6 can sustain more pressure than K_2YCuF_6 when the two compounds are compressed since its value of B (93.36) is greater than K_2YCuF_6's (34.87). K_2ScCuF_6 is therefore more resistant to external forces than K_2YCuF_6. It is clear from the table that K_2ScCuF_6 (37.76) has a larger shear modulus (G) than K_2YCuF_6 (12.31), indicating that the former is tougher than the latter. It must be noted that the values of B obtained by analyzing the elastic constants are seen to differ from those obtained from volumetric strain versus pressure (E − V) curve. One possible explanation for this apparent difference is that the two approaches used different measurement procedures.

Furthermore, stiffness of material is determined using Young's modulus (E), and the stiffness increases with larger values of E [49]. We conclude that K_2ScCuF_6 is stiffer than K_2YCuF_6 based on the calculated values of their young moduli 99.83 and 33.04, respectively.

Another significant factor is anisotropy that describes the directional dependency of material characteristics. The medium is isotropic if A = 1; otherwise, it is anisotropic [50]. By using the computed values shown in Table 2, one can determine the compounds' anisotropic behavior. For instance, the predicted values for K_2YCuF_6 (1.53) and K_2ScCuF_6 (0.30) deviate from unity, indicating that both compounds are anisotropic and that K_2YCuF_6 is more anisotropic than K_2ScCuF_6.

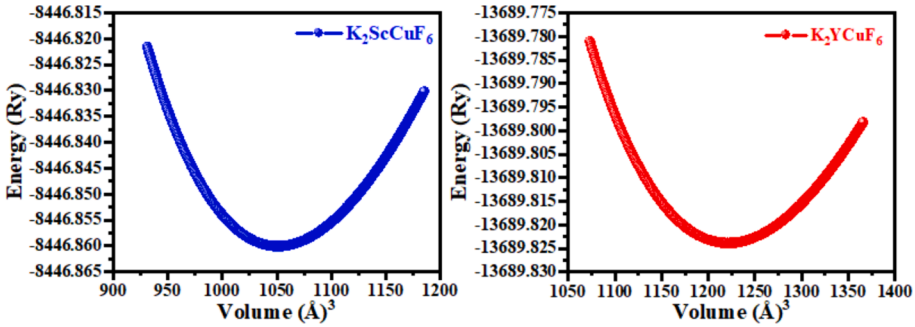

Fig. 2. Volume optimization curves of **(a)** K_2ScCuF_6 and **(b)** K_2YCuF_6.

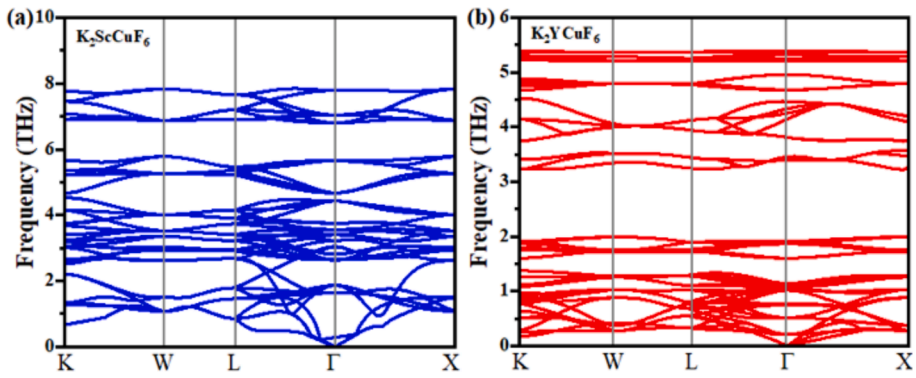

Fig. 3. Calculated phonon dispersion curves of **(a)** K_2ScCuF_6 and **(b)** K_2YCuF_6.

Table 2
Elastic Parameters of K_2ScCuF_6 and K_2YCuF_6.

Compounds	C_{11} (GPa)	C_{12} (GPa)	C_{44} (GPa)	A	B (GPa)	G_v	G_R	G	E	υ	B/G
K_2ScCuF_6	194.28	42.89	22.76	0.30	93.36	43.93	31.59	37.76	99.83	0.45	2.47
K_2YCuF_6	47.61	28.51	14.59	1.53	34.87	12.57	12.04	12.31	33.04	0.49	2.83

Another well-known measure of the tendency of a substance to experience lateral deformation in response to an axial strain is Poisson's ratio (*v*). In other words, a compound's ductile and brittle properties are determined by its Poisson ratio. Generally speaking, ductile behavior is indicated by a value higher than 0.26 [51]. Table 2 makes it obvious that K_2ScCuF_6 and K_2YCuF_6 are both ductile, with Poisson ratios of 0.45 and 0.49, respectively.

In a similar way, a material's flexibility may be ascertained by dividing its bulk modulus (B) by its shear modulus (G), or Pugh ratio. A compound's brittleness and ductility can be assessed using the Pugh ratio. In general, ductile materials possess a B/G ratio above 1.75 [52,53]. The estimated B/G (2.47 for K_2ScCuF_6 and 2.83 for K_2YCuF_6) indicate that both K_2ScCuF_6 and K_2YCuF_6 are ductile, while K_2YCuF_6 appears to be more ductile than K_2ScCuF_6. Thus, the mechanical properties conclude that the two compounds are ductile in nature.

Electronic properties

This section discusses the band structures and density of states (DOS) of K_2ScCuF_6 and K_2YCuF_6. The optical and electrical features of these materials are connected to their crystal structures through the analysis of band structures, which provides significant information of the conductivity characteristics of the compounds.

Fig. 4 shows the band structures of K_2ScCuF_6 and K_2YCuF_6, as determined by the TB-mBJ with spin orbit coupling (SOC) and without SOC. The two compounds' respective band structures of 1.2 eV and 2.3 eV make it obvious that they are semiconductors. The greater atomic size and less electronegativity of Y causes the band gap to expand when Y is substituted for Sc in K_2ScCuF_6, moving the minimum of conduction band farther from Fermi level. Beside this we also calculated the band structure by including the spin orbit coupling (SOC). From results it can be observed that by including the SOC the band gap decreases, it become 1.13 eV for K_2ScCuF_6 and 2.1 eV for K_2YCuF_6. Research on the production of these materials for solar cells is aided by this.

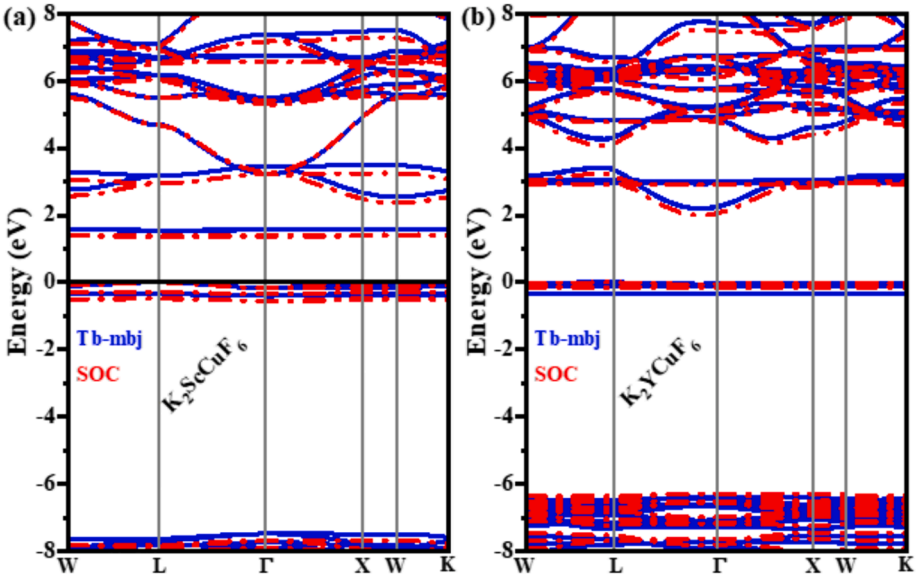

Fig. 4. Band structure with SOC and without SOC of double perovskites **(a)** $K_2ScCuCl_6$ and **(b)** K_2YCuCl_6.

The distribution of energy levels is described by the DOS and shows the characteristics of the band gap to help understand electrical behavior. The valence and conduction bands are separated Fermi energy (E_F), with valence band having filled low-energy levels while conduction band having vacant levels above E_F.

In Fig. 5, Sc/Y and halogen atoms significantly impact conduction band, whereas Cu and halogen atoms (F) mostly contribute to the valence band. The K contribution is also noticeable in the conduction band of the K_2YCuF_6 compound. This implies that Cu and halogen orbitals give birth to occupied energy levels, while Y/Sc orbitals are the source of unoccupied energy levels.

Optical properties

An optical characteristic is the way a material interacts with light, and it is very important in optoelectronics, photonics, and optics. The dielectric function, refractive index, refraction, reflection, optical conductivity and absorption are the examples of fundamental characteristics. The obtained $\varepsilon_1(\omega)$ and ε_2 (ω) of the two compounds within energy range of 0 eV to 14 eV of incoming photon are displayed in Fig. 6. Wave damping and energy dissipation are represented by $\varepsilon_1(\omega)$, whereas polarization and energy storage are represented by $\varepsilon_2(\omega)$. In comparison to K_2YCuF_6 (1.36), K_2ScCuF_6 dissipates more energy (2.18), according to static dielectric function $\varepsilon_1(0)$. The compounds had maximum values of $\varepsilon_2(\omega)$ of 3.4 at 8.15 eV and 2.3 at 9.8 eV, respectively.

Refractive index is a property of materials that depends on composition and structure to determine how light passes through them. The $\varepsilon_1(\omega)$ and $\varepsilon_2(\omega)$ values derived from dielectric function are utilized to determine a material's refractive index. The refractive indices for K_2ScCuF_6 and K_2YCuF_6 are given in Fig. 7(a). The static refractive index n(0), for K_2ScCuF_6 and K_2YCuF_6 are 1.47 and 1.17, respectively. K_2ScCuF_6 has 2.01 peak value at about 8.04 eV of photon energy, according to n(ω) spectrum, whereas K_2YCuF_6 shows 1.75 peak value at approximately 9.72 eV. In applications involving light refraction, especially in photoelectric applications, n(0) is significant. When n(ω) is greater than 1, photons interact with electrons and slow down when they enter a material. This results in prolonging the time it takes for the photons to pass through the material. The rise of electrical density of a substance can also causes its refractive index to rise.

The calculated reflectivity R (ω) of K_2ScCuF_6 and K_2YCuF_6, given in Fig. 7(b). At zero frequency R(0), the reflectance of K_2ScCuF_6 is 0.37, whereas that of K_2YCuF_6 is 0.0059. Both compounds exhibit a rise in reflectance with photon energy increase. At around 13.56 eV, they achieve their highest reflectivity of 0.48 and 0.25, respectively. In the observed energy range, K_2ScCuF_6 and K_2YCuF_6 both show exceptionally low reflectance. These are highly transparent to the incoming photons because of their low level of reflectance, which is compatible with their band gap. These materials are promising because of their great

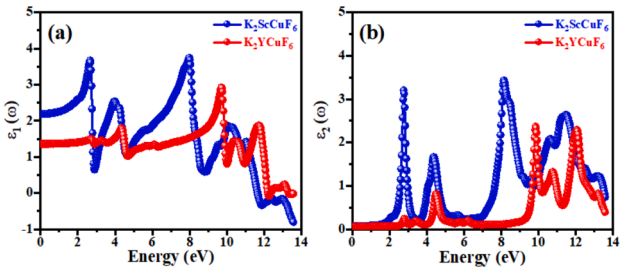

Fig. 6. Calculated **(a)** $\varepsilon_1(\omega)$ and **(b)** $\varepsilon_2(\omega)$ of K_2ScCuF_6 and K_2YCuF_6.

transparency, which is favorable for uses like solar cells and optics, where effective light transmission is required. The absorbance curves obtained for the chosen compounds K_2ScCuF_6 and K_2YCuF_6 by the ε(ω) method are shown in Fig. 7(c). Significant absorption is seen by these materials in 0 to 14 eV energy range. The absorption thresholds indicate the point at which certain materials start to absorb electromagnetic radiation, and they are found at 0 eV. K_2YCuF_6 has a maximum absorption of 119.47 at 12.15 eV photon energy value, whereas K_2ScCuF_6 shows a maximum absorption value of 132.48 at 13.56 eV. This illustrates the degree to which particular substances may absorb light within a specified energy range.

In Fig. 7(d), highest optical conductivity value of K_2ScCuF_6 is about 3981 Ω^{-1} cm^{-1} at 11.5 eV, whereas K_2YCuF_6 displays a significant value of around 3621 Ω^{-1} cm^{-1} at 12.0 eV. This suggests that certain substances, particularly at higher energies, exhibit outstanding optical conductivity. They are attractive options for use in telecommunications, photonics and other cutting-edge optoelectronic technologies due to their advantageous optical conductivity properties [54].

Conclusion

The structural, electronic, optical, and elastic characteristics of the double perovskite compounds K_2ScCuF_6 and K_2YCuF_6 are investigated by the using DFT simulations. The fitted curve for the Birch Murnaghan equation of state (EOS) and negative formations energy indicate that both structures are stable and can fabricated. Furthermore, it is observed that K_2ScCuF_6 has a higher bulk modulus compared to K_2YCuF_6. K_2ScCuF_6 and K_2YCuF_6 compounds have 1.2 and 2.3 eV small band gaps, respectively, which are revealed by analyzing the electronic properties via precise TB-mBJ approximation. In addition, mechanical analysis revealed ductile, anisotropic and mechanical stability of the compounds. Through optical studies, one can acquire a thorough insight of the compounds' behavior in numerous areas of their characteristics, including transparency at lower energy values and notable transmission and absorption at higher energies. These interesting results imply that K_2ScCuF_6 and K_2YCuF_6 have significant potential in solar cells, light-

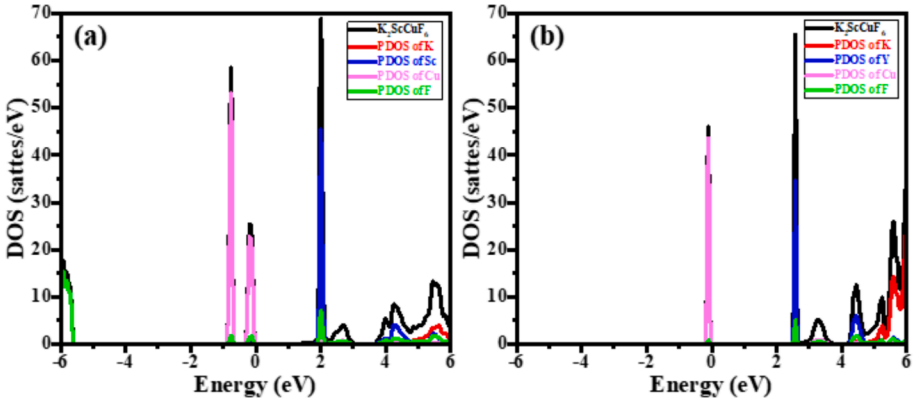

Fig. 5. Calculated DOS of double perovskites **(a)** K_2ScCuF_6 and **(b)** K_2YCuF_6.

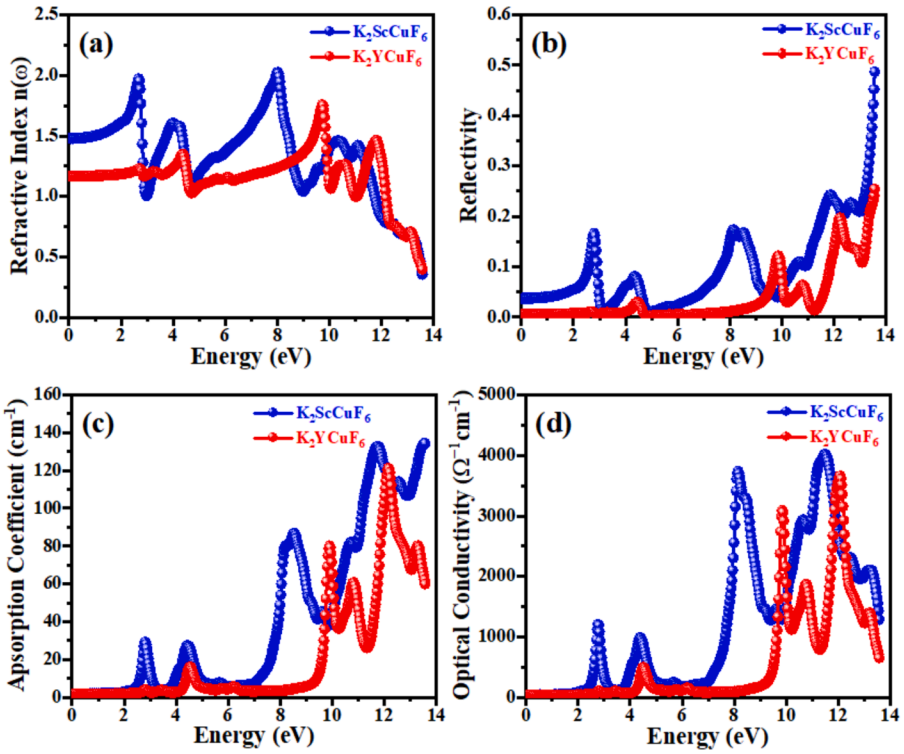

Fig. 7. Calculated **(a)** refractive index n(ω) **(b)** reflectivity R(ω) **(c)** absorption α(ω) and **(d)** conductivity σ(ω) of double perovskites K_2ScCuF_6 and K_2YCuF_6.

emitting diodes (LEDs), smart windows, displays and sensors.

CRediT authorship contribution statement

Amina: Writing – original draft, Writing – review & editing, Supervision. **Muhammad Uzair:** Supervision, Resources. **Amir Sohail Khan:** Methodology, Data curation. **A.M. Quraishi:** Formal analysis, Conceptualization. **Albandary Almahri:** Formal analysis, Data curation. **Mukhlisa Soliyeva:** Validation, Data curation. **Vineet Tirth:** Writing – review & editing, Writing – original draft, Conceptualization. **Ali Algahtani:** Writing – review & editing, Writing – original draft, Conceptualization. **Abdullah:** Writing – review & editing, Resources, Methodology. **Rawaa M. Mohammed:** Visualization, Validation. **Mahidur R. Sarker:** Formal analysis, Conceptualization. **N.M.A. Hadia:** Software, Resources. **Abid Zaman:** Writing – review & editing, Software, Conceptualization.

Declaration of competing interest

The authors declare that they have no known competing financial interests or personal relationships that could have appeared to influence the work reported in this paper.

Data availability

Data will be made available on request.

Acknowledgments

The authors extend their appreciation to the Deanship of Scientific Research at King Khalid University Abha 61421, Asir, Kingdom of Saudi Arabia for funding this work through the Large Groups Project under grant number RGP.2/545/45. This research was funded by the Universiti Kebangsaan Malaysia under Grant Code GP-K023619.

References

[1] Wang D, Wang XX, Jin ML, He P, Zhang S. Molecular level manipulation of charge density for solid-liquid TENG system by proton irradiation. Nano Energy 2022;103:107819.
[2] Wang M, Jiang C, Zhang S, Song X, Tang Y, Cheng HM. Reversible calcium alloying enables a practical room-temperature rechargeable calcium-ion battery with a high discharge voltage. Nat Chem 2018;10(6):667–72.
[3] Chen XF. Periodic density functional theory (PDFT) simulating crystal structures with microporous CHA framework: an accuracy and efficiency study. Inorganics 2023;11(5):215.
[4] Zhang X, Tang Y, Zhang F, Lee CS. A novel aluminum–graphite dual-ion battery. Adv Energy Mater 2016;6(11):1502588.
[5] Chen X, Yu T. Simulating crystal structure, acidity, proton distribution, and IR spectra of acid zeolite HSAPO-34: a high accuracy study. Molecules 2023;28(24):8087.
[6] Ye S, Zhu J, Zhu S, Zhao Y, Li M, Huang Z, et al. Design strategies for perovskite-type high-entropy oxides with applications in optics. ACS Appl Mater Interfaces 2023;15(40):47475–86.
[7] Wang Z, Fu W, Hu L, Zhao M, Guo T, Hrynsphan D, et al. Improvement of electron transfer efficiency during denitrification process by Fe-Pd/multi-walled carbon nanotubes: possessed redox characteristics and secreted endogenous electron mediator. Sci Total Environ 2021;781:146686.
[8] Luo ZZ, Cai S, Hao S, Bailey TP, Luo Y, Luo W, et al. Extraordinary role of Zn in enhancing thermoelectric performance of Ga-doped n-type PbTe. Energ Environ Sci 2022;15(1):368–75.
[9] Lu Y, Stegmaier M, Nukala P, Giambra MA, Ferrari S, Busacca A, et al. Mixed-mode operation of hybrid phase-change nanophotonic circuits. Nano Lett 2017;17(1):150–5.
[10] Husain M, Rahman N, Azzouz-Rached A, Tirth V, Ullah H, Elhadi M, et al. Exploring silicon-based Ca2TiSiO6 ordered double perovskite oxides: a comprehensive DFT investigation of structural, dynamical, mechanical stability, and optoelectronic properties. Silicon 2024:1–10.
[11] Bibi S, Husain M, Tirth V, Ahmed SB, Rahman N, Azzouz-Rached A, et al. Insight into the physical properties of Rb2YCuX6 (X= Br and I) lead-free elpasolite for high-energy applications. Phys Scr 2024;99(3):035906.
[12] Rahman N, Husain M, Tirth V, Azzouz-Rached A, Bibi S, Inayat K, et al. Insight into the structural, elastic, phonon dispersions, and optoelectronic properties of Cs2YXCl6 (X= In, Tl) double perovskites for solar cells and energy conversion applications. Optik 2024;299:171590.
[13] Slavney AH, Hu T, Lindenberg AM, Karunadasa HI. A bismuth-halide double perovskite with long carrier recombination lifetime for photovoltaic applications. J Am Chem Soc 2016;138(7):2138–41.
[14] Lu C, Ren R, Zhu Z, Pan G, Wang G, Xu C, Sun K. (2023). BaCo0. 4Fe0. 4Nb0. 1Sc0. 1O3-δ perovskite oxide with super hydration capacity for a high-activity proton ceramic electrolytic cell oxygen electrode. Chemical Engineering Journal, 472, 144878.

[15] Giustino F, Snaith HJ. Toward lead-free perovskite solar cells. ACS Energy Lett 2016;1(6):1233–40.
[16] Zhang Z, Su J, Hou J, Lin Z, Hu Z, Chang J, et al. Potential applications of halide double perovskite Cs2AgInX6 (X= Cl, Br) in flexible optoelectronics: unusual effects of uniaxial strains. The Journal of Physical Chemistry Letters 2019;10(5):1120–5.
[17] Zelewski SJ, Urban JM, Surrente A, Maude DK, Kuc A, Schade L, et al. Revealing the nature of photoluminescence emission in the metal-halide double perovskite Cs 2 AgBiBr 6. J Mater Chem C 2019;7(27):8350–6.
[18] Huang Z, Zhang Y, Wang H, Li J. Improved electrical resistivity-temperature characteristics of oriented hBN composites for inhibiting temperature-dependence DC surface breakdown. Appl Phys Lett 2023;123(10):103501.
[19] Jiang C, Deng Z, Liu B, Li J, Han Z, Ma Y, et al. Spin–orbit-engineered selective transport of photons in plasmonic nanocircuits with panda-patterned transporters. ACS Photonics 2022;9(9):3089–93.
[20] Lee MM, Teuscher J, Miyasaka T, Murakami TN, Snaith HJ. Efficient hybrid solar cells based on meso-superstructured organometal halide perovskites. Science 2012;338(6107):643–7.
[21] Kim HS, Lee CR, Im JH, Lee KB, Moehl T, Marchioro A, et al. Lead iodide perovskite sensitized all-solid-state submicron thin film mesoscopic solar cell with efficiency exceeding 9%. Sci Rep 2012;2(1):591.
[22] Qiao G, Zeng Z, Gao J, Tang Y, Wang Q. An efficient route to assemble novel organometal halide perovskites and emission evolution performance. J Alloy Compd 2019;771:418–23.
[23] Liu X, Gao J, Liu W, Wang Q. Reinforcing effects of waterproof substrate on the photo-, thermal and pH stabilities of perovskite nanocrystals. J Alloy Compd 2020;817:152693.
[24] Kong L, Liu Y, Dong L, Zhang L, Qiao L, Wang W, et al. Enhanced red luminescence in CaAl 12 O 19: Mn 4+ via doping Ga 3+ for plant growth lighting. Dalton Trans 2020;49(6):1947–54.
[25] Ajia IA, Edwards PR, Pak Y, Belekov E, Roldan MA, Wei N, et al. Generated carrier dynamics in V-pit-enhanced InGaN/GaN light-emitting diode. ACS Photonics 2017;5(3):820–6.
[26] Saliba M, Matsui T, Domanski K, Seo JY, Ummadisingu A, Zakeeruddin SM, et al. Incorporation of rubidium cations into perovskite solar cells improves photovoltaic performance. Science 2016;354(6309):206–9.
[27] Shao S, Liu J, Portale G, Fang HH, Blake GR, ten Brink GH, et al. Highly reproducible Sn-based hybrid perovskite solar cells with 9% efficiency. Adv Energy Mater 2018;8(4):1702019.
[28] Kopacic I, Friesenbichler B, Hoefler SF, Kunert B, Plank H, Rath T, et al. Enhanced performance of germanium halide perovskite solar cells through compositional engineering. ACS Appl Energy Mater 2018;1(2):343–7.
[29] Wang N, Zhou Y, Ju MG, Garces HF, Ding T, Pang S, et al. Heterojunction-depleted lead-free perovskite solar cells with coarse-grained B-γ-CsSnI3 thin films. Adv Energy Mater 2016;6(24):1601130.
[30] Jiang X, Li H, Zhou Q, Wei Q, Wei M, Jiang L, et al. One-step synthesis of SnI2·(DMSO) x adducts for high-performance tin perovskite solar cells. J Am Chem Soc 2021;143(29):10970–6.
[31] McClure ET, Ball MR, Windl W, Woodward PM. Cs2AgBiX6 (X= Br, Cl): new visible light absorbing, lead-free halide perovskite semiconductors. Chem Mater 2016;28(5):1348–54.
[32] Wolf NR, Connor BA, Slavney AH, Karunadasa HI. Doubling the stakes: the promise of halide double perovskites. Angew Chem 2021;133(30):16400–14.
[33] Greul E, Petrus ML, Binek A, Docampo P, Bein T. Highly stable, phase pure Cs 2 AgBiBr 6 double perovskite thin films for optoelectronic applications. J Mater Chem A 2017;5(37):19972–81.
[34] Uddin MS, Hossain MK, Uddin MB, Toki GF, Ouladsmane M, Rubel MH, et al. An in-depth investigation of the combined optoelectronic and photovoltaic properties of lead-free Cs2AgBiBr 6 double perovskite solar cells using DFT and SCAPS-1D frameworks. Adv Electron Mater 2024;10(5):2300751.
[35] Rubel MHK, Hossain MA, Hossain MK, Hossain KM, Khatun AA, Rahaman MM, et al. First-principles calculations to investigate structural, elastic, electronic, thermodynamic, and thermoelectric properties of CaPd3B4O12 (B= Ti, V) perovskites. Results Phys 2022;42:105977.
[36] Hossain MK, Samajdar DP, Das RC, Arnab AA, Rahman MF, Rubel MHK, et al. Design and simulation of Cs2BiAgI6 double perovskite solar cells with different electron transport layers for efficiency enhancement. Energy Fuel 2023;37(5):3957–79.
[37] Hossain MK, Arnab AA, Samajdar DP, Rubel MHK, Hossain MM, Islam MR, et al. Design insights into La2NiMnO6-based perovskite solar cells employing different charge transport layers: DFT and SCAPS-1D frameworks. Energy Fuel 2023;37(17):13377–96.
[38] Bouhmaidi S, Uddin MB, Pingak RK, Ahmad S, Rubel MHK, Hakamy A, et al. Investigation of heavy thallium perovskites TlGeX3 (X= Cl, Br and I) for optoelectronic and thermoelectric applications: A DFT study. Mater Today Commun 2023;37:107025.
[39] Hossain MK, Toki GI, Samajdar DP, Mushtaq M, Rubel MHK, Pandey R, et al. Deep insights into the coupled optoelectronic and photovoltaic analysis of lead-free CsSnI3 perovskite-based solar cell using DFT calculations and SCAPS-1D simulations. ACS Omega 2023;8(25):22466–85.
[40] Obot I, Macdonald DD, Gasem Z. Density functional theory (DFT) as a powerful tool for designing new organic corrosion inhibitors: Part 1: An overview. Corros Sci 2015;99:1–30.
[41] Blaha P, Schwarz K, Madsen GKH, Kuasnicke D, Luitz J. Introduction to WIEN2K. An Augmented plane wane plus local orbitals program for calculating crystal properties. Vienna, Austria: Vienna university of technology; 2001.
[42] Katsura T, Tange Y. A simple derivation of the Birch-Murnaghan equations of state (EOSs) and comparison with EOSs derived from other definitions of finite strain. Minerals 2019;9(12):745.
[43] Kadim G, Masrour R, Jabar A. A comparative study between GGA, WC-GGA, TB-mBJ and GGA+ U approximations on magnetocaloric effect, electronic, optic and magnetic properties of BaMnS2 compound: DFT calculations and Monte Carlo simulations. Phys Scr 2021;96(4):045804.
[44] Tran F, Blaha P. Accurate band gaps of semiconductors and insulators with a semilocal exchange-correlation potential. Phys Rev Lett 2009;102(22):226401.
[45] Glazer AM. WINOPTACT: a computer program to calculate optical rotatory power and refractive indices from crystal structure data. J Appl Cryst 2002;35(5):652.
[46] Rahaman MM, Hossain KM, Rubel MHK, Islam AA, Kojima S. Alkaline-Earth metal effects on physical properties of ferromagnetic AVO3 (A= Ba, Sr, Ca, and Mg): density functional theory insights. ACS Omega 2022;7(24):20914–26.
[47] Khandy SA, Gupta DC. Structural, elastic and thermo-electronic properties of paramagnetic perovskite PbTaO 3. RSC Adv 2016;6(53):48009–15.
[48] Ghebouli B, Ghebouli MA, Bouhemadou A, Fatmi M, Khenata R, Rached D, et al. Theoretical prediction of the structural, elastic, electronic, optical and thermal properties of the cubic perovskites CsXF3 (X= Ca, Sr and Hg) under pressure effect. Solid State Sci 2012;14(7):903–13.
[49] Hossain MK, Toki GI, Kuddus A, Rubel MHK, Hossain MM, Bencherif H, et al. An extensive study on multiple ETL and HTL layers to design and simulation of high-performance lead-free CsSnCl3-based perovskite solar cells. Sci Rep 2023;13(1):2521.
[50] Yang Y, Lu H, Yu C, Chen JM. First-principles calculations of mechanical properties of TiC and TiN. J Alloy Compd 2009;485(1–2):542–7.
[51] Khan NU, Khan UA, Zaman A, Algahtani A, Al-Humaidi JY, Tirth V, et al. Insight into structural, electronic, optical and elastic properties of double perovskites Rb2XCrCl6 (X= K, Na) via DFT study. J Phys Chem Solid 2023;181:111479.
[52] Pugh SF. XCII. Relations between the elastic moduli and the plastic properties of polycrystalline pure metals. The London, Edinburgh, and Dublin Philosophical Magazine and Journal of Science 1954;45(367):823–43.
[53] Khan UA, Ullah I, Tirth V, Algahtani A, Zaman A. DFT study of the structural, elastic and optoelectronic properties of Cu-based cubic halide-perovskites ACuF3 (A= Mg and Ca). Phys Scr 2022;97(8):085819.
[54] Hossain MK, Toki GI, Alam I, Pandey R, Samajdar DP, Rahman MF, et al. Numerical simulation and optimization of a CsPbI 3-based perovskite solar cell to enhance the power conversion efficiency. New J Chem 2023;47(10):4801–17.